AD-A088 107 NAVAL RESEARCH LAB WASHINGTON DC F/G 7/4
XUV ALUMINUM SPECTRA OF LASER-PRODUCED PLASMAS.(U)
JUL 80 G A DOSCHEK, U FELDMAN
UNCLASSIFIED NRL-8416 NL

END
DATE FILMED
9-80
DTIC

(12) LEVEL II

(14) NRL [redacted] 8416

AD A088107

(6) **XUV Aluminum Spectra of Laser-Produced Plasmas**

(10) G. A. Doschek [redacted] U. Feldman

E. O. Hulburt Center for Space Research
Space Science Division

(9) Interim rept.,

(11) 15 Jul [redacted] 80

(12) 15

(16) RR011109

(17) RR011094 1

NAVAL RESEARCH LABORATORY
Washington, D.C.

251950

SECURITY CLASSIFICATION OF THIS PAGE (When Data Entered)

REPORT DOCUMENTATION PAGE

READ INSTRUCTIONS BEFORE COMPLETING FORM

1. REPORT NUMBER: NRL Report 8416
2. GOVT ACCESSION NO.: AD-A088 107
3. RECIPIENT'S CATALOG NUMBER:

4. TITLE (and Subtitle): XUV ALUMINUM SPECTRA OF LASER-PRODUCED PLASMAS
5. TYPE OF REPORT & PERIOD COVERED: Interim report on a continuing problem
6. PERFORMING ORG. REPORT NUMBER:

7. AUTHOR(s): G. A. Doschek and U. Feldman
8. CONTRACT OR GRANT NUMBER(s):

9. PERFORMING ORGANIZATION NAME AND ADDRESS: Naval Research Laboratory, Washington, DC 20375
10. PROGRAM ELEMENT, PROJECT, TASK AREA & WORK UNIT NUMBERS: RR0110941; 71-0974-0-0

11. CONTROLLING OFFICE NAME AND ADDRESS: Department of the Navy, Office of Naval Research, Arlington, VA 22217
12. REPORT DATE: July 15, 1980
13. NUMBER OF PAGES: 14

14. MONITORING AGENCY NAME & ADDRESS(if different from Controlling Office):
15. SECURITY CLASS. (of this report): UNCLASSIFIED
15a. DECLASSIFICATION/DOWNGRADING SCHEDULE:

16. DISTRIBUTION STATEMENT (of this Report)

Approved for public release, distribution unlimited

17. DISTRIBUTION STATEMENT (of the abstract entered in Block 20, if different from Report)

18. SUPPLEMENTARY NOTES

19. KEY WORDS (Continue on reverse side if necessary and identify by block number)

XUV spectroscopy
Laser produced plasma

20. ABSTRACT (Continue on reverse side if necessary and identify by block number)

XUV aluminum spectra from 200 to 500 Å of laser-produced plasmas are discussed. The plasmas were obtained by focusing Nd:glass and CO_2 laser pulses onto planar targets. The spectrograph was a normal incidence instrument without an entrance slit. Therefore monochromatic images of the plasma are formed at the focal plane, rather than spectral lines. Kodak 101 film was used to record the spectra. Images of the plasmas due to transitions in Al V through Al X were identified using a theoretical synthetic aluminum spectrum. The time- and space-integrated relative numbers of the ions from Al V through Al X can be obtained from a comparison of the synthetic and laser-plasma spectra. The

next page
(Continues)

DD FORM 1 JAN 1473 EDITION OF 1 NOV 65 IS OBSOLETE
S/N 0102-014-6601

SECURITY CLASSIFICATION OF THIS PAGE (When Data Entered)

20. Abstract (Continued)

comparison enables determination of the film calibration curve and the efficiency of the instrument with wavelength. The morphology of the expansion of the plasma is also discussed. The plasma of the highest temperature ions (Al X) expands outward in cylindrically shaped structures. The expansion of the lower temperature plasma (such as Al VII) is also cylindrical in appearance, but the images are not as tightly confined to the target normal as for the hotter ions.

CONTENTS

XUV ALUMINUM SPECTRA OF LASER-PRODUCED PLASMAS

INTRODUCTION

We have obtained extreme-ultraviolet (XUV) spectra of plasmas produced by focusing Nd:glass and CO_2 laser pulses onto solid planar targets [1,2]. The spectra were recorded in the region from 200 to 500 Å using a slitless spectrograph. Because of the absence of a slit, monochromatic images of the plasma, rather than spectral lines, are formed at the focal plane of the instrument. The dispersing element was a concave spherical gold-coated Bausch and Lomb replica grating with 3600 lines per millimeter. The spectral images were recorded on Kodak 101 film. Therefore the spectra are time-integrated over the lifetimes of the plasmas. A schematic layout of the instrument and the theoretical efficiency of the instrument as a function of wavelength are given in Ref. 1. The setup for the glass-laser experiment also is described in Ref. 1. The CO_2-laser experiment is described in Ref. 2.

For the glass-laser experiment, an approximately-10-J pulse of 1.06-μm radiation was delivered onto the target in times varying from 100 to 500 ps. Most of the energy was focused into a 20-μm-diameter spot on the flat target surface. For the CO_2-laser experiment, approximately 60 J of 10.6-μm radiation was delivered within a 200-μm focal spot on the target. The CO_2 pulse consisted of a gain switch spike of 70-ns duration (FWHM) and a tail of 1-μs duration. Approximately 1/3 of the total energy was contained within the spike.

The targets and spectrograph were enclosed in vacuum. In both experiments plasma could be detected as far as 1 cm from the target surface. A variety of target materials were chosen, including metals such as iron, aluminum, and titanium as well as lighter substances such as graphite. Most of the targets were flat thick slabs. In a few cases, however, thin foils were used. In particular, in this report we discuss the spectrum of an aluminum-foil plasma produced by a glass laser. In this experiment, an aluminum layer 100 μm thick was deposited on a paralene substrate about 10 μm thick.

In Refs. 1 and 2 we discussed the morphology of the expanding plasmas obtained using various target materials and determined the electron density in different regions of the plasmas using the relative intensities of different spectral images. These latter results were based on an analysis of the populations of the ground state and certain excited levels of the ions Ti XII and Fe XVI. In this report we discuss the aluminum-foil spectrum obtained using the glass laser and qualitatively compare the glass-laser spectrum to a spectrum obtained from the CO_2 laser using a thick aluminum target. We show that this type of analysis can be used to derive the time-integrated relative number densities of Al V through Al X in the plasma region near the target surface. The result could be refined by repeating the analysis for spectra produced using, for example, silicon or magnesium targets.

Manuscript submitted April 15, 1980.

THE EXPERIMENTAL SPECTRA

Figure 1 shows the spectrum of the aluminum-foil plasma produced by the glass laser and the spectrum of the thick-slab plasma produced by the CO_2 laser. Also shown is a theoretical spectrum that will be discussed shortly. The wavelength range for these spectra is 250 to 440 Å. Within this range aluminum emission lines are produced by transitions between the $2s^2 2p^k$, $2s2p^{k+1}$, and $2p^{k+2}$ configurations in the ions from Al V through Al X.

The CO_2-laser-produced spectrum is oriented such that the laser pulse was incident from the bottom to the top of Fig. 1. The rather faint emission in the horizontal strip near the top of the spectrum is due to continuum emission close to the target surface. The plasma expands downward from the target surface in rather narrow conical plumes. A scale giving distances at the target is shown to the right of the spectrum. The spectral images of the plasma produced by the Nd:glass laser shown below the CO_2-laser-produced spectrum differ from the CO_2-laser-produced images, for two possible reasons. First, because a foil only 100 nm thick was used, not much solid aluminum was available for conversion to plasma relative to the amount available from the thick target used to generate the CO_2-laser-produced spectrum. Second, the images produced using the glass laser were usually not extended like the images produced using the CO_2 laser. This may be due to the much longer pulse length of the CO_2 laser. The glass-laser-produced spectrum in Fig. 1 is oriented in the opposite sense from the CO_2-laser-produced spectrum. The laser pulse is incident on the target from top to bottom in the figure, and the target was inclined at a slight angle to the incident radiation.

The usefulness of the foil spectrum becomes apparent by comparing the images in both spectra with the theoretical spectrum. Many of the lines are clearly resolved in only the foil spectrum. Even in this spectrum quite a few of the images are blends of several emission lines, sometimes from different ionization stages. Hence we use the foil spectrum for a quantitative comparison between experiment and theory.

THE THEORETICAL SPECTRA

Recently there has been considerable theoretical work on the electron impact excitation of positive ions of the elements lighter than cobalt. The impetus for this work is newly acquired rather-high-quality spectra of the solar atmosphere, primarily recorded by spectrographs flown on the Skylab manned space station. One NRL instrument on Skylab was a slitless spectrograph quite similar to the laboratory instrument used in our laser experiments. This instrument was useful for recording spectral images of solar flares between 170 and 600 Å. In this wavelength range, solar emission lines are present that originate in regions of the solar atmosphere that span a temperature range from about 2 eV to about 2 keV. Most of these lines originate from transitions between the $2s^2 2p^k$ and $2s2p^{k+1}$ configurations of highly ionized ions. These lines are also strong in higher density laser-produced plasmas, but in addition strong lines are also present in laser spectra due to transitions between the $2s2p^{k+1}$ and $2p^{k+2}$ configurations. The reason for this is the much higher electron density in laboratory plasmas, which we have discussed in detail elsewhere [1].

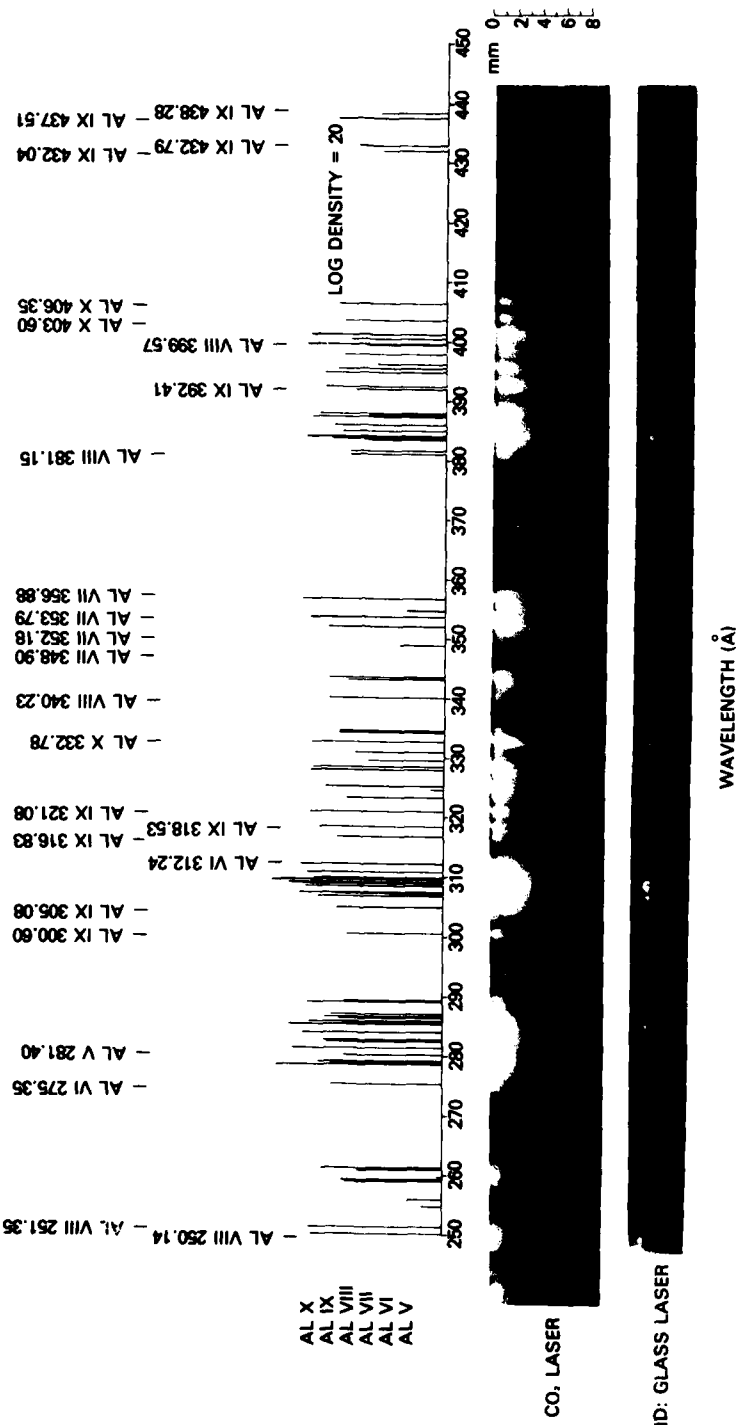

Fig. 1 — Laser-produced-plasma spectra of aluminum targets, compared with a theoretical synthetic spectrum. A thick target was used for the CO_2-laser experiment, and a foil target was used for the glass-laser experiment.

The solar calculations were done for ions of the elements that are abundant in the solar atmosphere: C, N, O, Ne, Mg, Si, S, Ar, Ca, Fe, and Ni. However, because the calculations now exist for most of these elements, it is relatively simple to interpolate or extrapolate and obtain results for nonsolar abundant ions with atomic number Z between carbon and nickel. It is difficult to cite a single reference for all the solar calculations. They are distributed quite widely in the solar and astrophysical literature. The papers by Dere et al. [3] and Feldman and Doschek [4] give a fair number of references to the recent work. In addition, we have unpublished calculations kindly supplied to us by A. K. Bhatia at the Goddard Space Flight Center, D. R. Flower now at the University of Durham, and H. E. Mason at Cambridge University.

The atomic calculations consist of electron-impact-excitation collision strengths and corresponding spontaneous radiative decay rates. The collision strengths were calculated at various energies of the perturbing electron for transitions between levels of the $2s^2 2p^k$, $2s2p^{k+1}$, and $2p^{k+2}$ configurations. In particular, because transitions between the $2s2p^{k+1}$ and $2p^{k+2}$ levels are not strong in solar spectra, most of the atomic data for these transitions are not published and have been made available to us privately by the workers mentioned.

The rate coefficients C_{ij}^e (cm^3-s^{-1}) for excitation between lower level i and upper level j are related to the collision strengths Ω_{ij} by the equation

$$C_{ij}^e = \frac{8.63 \times 10^{-6}}{\omega_i k T_e^{3/2}} \int_{\Delta E_{ij}}^{\infty} \Omega_{ij}(\mathrm{E}) e^{-E/kT_e}\, dE, \tag{1}$$

where ω_i is the statistical weight of the lower level, T_e is the electron temperature (K), k is Boltzmann's constant, and ΔE_{ij} is the transition energy. Equation (1) assumes a Maxwellian electron distribution. The intensity I_{ij} (ergs-cm^{-2}-s^{-1}-st^{-1}) in a particular line is given by

$$I_{ij} = \frac{\Delta E_{ij}}{4\pi} A_{ji} \int_{\Delta h} N_j\, dh, \tag{2}$$

where A_{ji} is the transition probability, h is the line of sight to the spectrograph, and N_j is the population (cm^{-3}) of the upper level j of the transition. The populations N_j are found by solving the coupled equations of statistical equilibrium:

$$N_j \left[\sum_{i<j} A_{ji} + N_e \left(\sum_{i>j} C_{ji}^e + \sum_{i<j} C_{ji}^d \right) \right] = N_e \left(\sum_{i<j} N_i C_{ij}^e + \sum_{i>j} N_i C_{ij}^d \right) + \sum_{i>j} N_i A_{ij} . \tag{3}$$

In Eqs. (3) C^d is the electron deexcitation rate, which is related to the excitation rate through the expression

$$C_{ji}^{d} = \frac{\omega_i}{\omega_j} C_{ij}^{e} e^{\Delta E_{ij}/kT_e}. \tag{4}$$

We assume in solving Eqs. (3) for application to the aluminum spectra that only excitations between levels with principal quantum number $n = 2$ are important. This is true for low densities ($N_e \lesssim 10^{17}$ cm^{-3}). At higher densities the $n = 2$ levels are nearly in Boltzmann equilibrium with each other. The atomic data for aluminum were extrapolated from the atomic data for silicon and sulfur.

In plotting the synthetic aluminum spectra, we have used experimental energy levels. Thus a real spectrum is obtained in the sense that the lines have correct wavelengths and can be plotted as in Fig. 1 and compared directly to experiment. (Atomic physicists use theoretical energy levels in calculating collision strengths and transition probabilities. These energy levels are usually within about 10% of the actual levels.) Finally, synthetic spectra can be generated for each ion assuming a range of values for T_e and N_e.

DISCUSSION

The foil spectrum shown in Fig. 1 was densitometered with a Grant microdensitometer. The densitometer slit size was set such that the entire dense core region of emission was covered. The electron densities of glass-laser-produced plasmas can range between 10^{18} cm^{-3} and 10^{21} cm^{-3} [1,5]. The lowest densities occur rather far from the target, where the emission is weak. A portion of the densitometered spectrum between 310 and 360Å is shown Fig. 2. Also shown are three theoretical spectra characterized by different electron densities. The widths of the theoretical spectral lines were determined by assuming that each ion emits at the temperature at which it is formed in ionization equilibrium. The ion temperature is assumed equal to the electron temperature, and the ionization equilibrium of Landini and Fossi [6] was used. The widths of the experimental images are determined by the spatial extent of the emission, which is much larger than the Doppler widths. The slight asymmetry of the experimental images occurred because the target was tilted at a small angle to the incoming laser pulse.

It is now appropriate to discuss one final aspect of the theoretical spectra. Equations (3) allow N_j to be determined for each aluminum ion, and I_{ij} can therefore be found for each line emitted by each ion. However, to calculate a synthetic spectrum such as shown in Fig. 1, it is still necessary to determine the relative population densities of the different ions, so that, for example, the intensities of the Al IX lines can be determined relative to the Al VIII and Al X lines. Actually, since the spectra we are measuring are time-integrated, the time-integrated intensity J_{ij}^{z} of a line from an ion of charge z as measured through the densitometer is given by

$$J_{ij}^{z} = \frac{\Delta E_{ij}}{4\pi} A_{ji} \frac{1}{A_d} \int dV \int dt\, N_j[x, y, h, N_e(t), T_e(t), t], \tag{5}$$

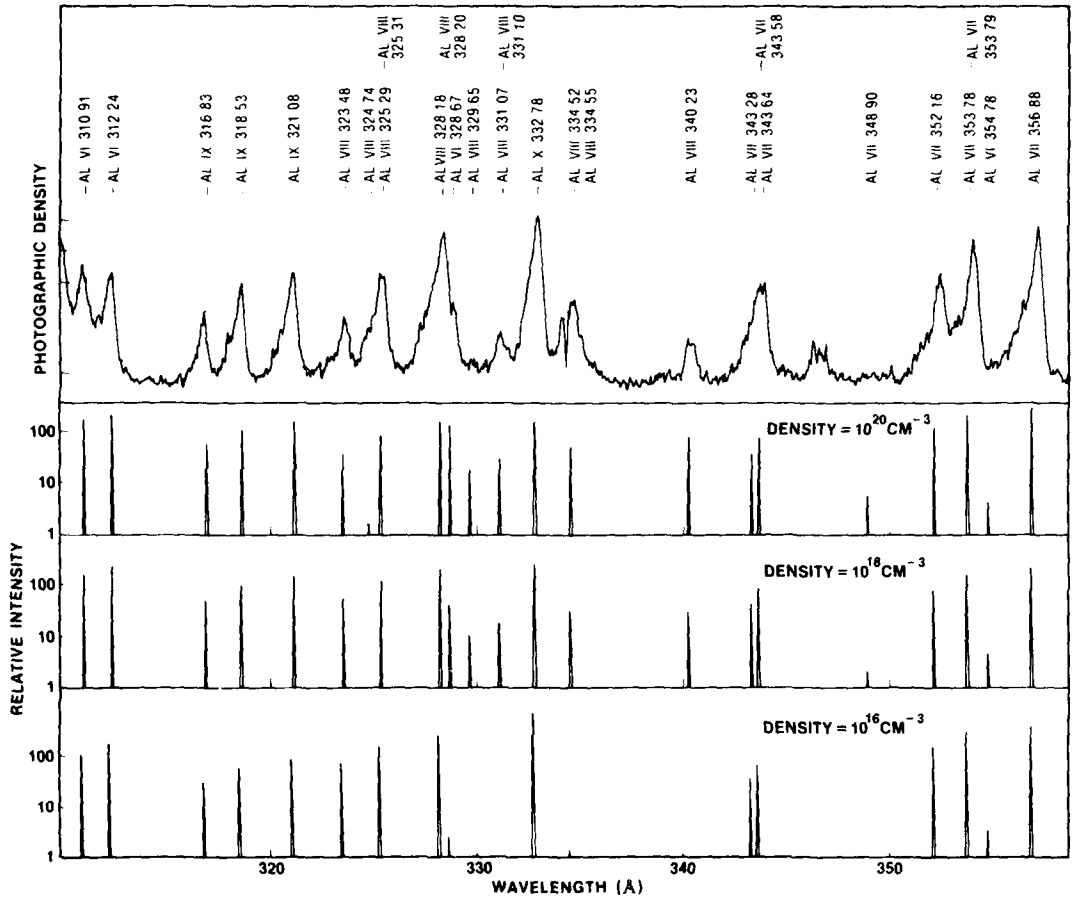

Fig. 2 — A densitometered portion of the glass-laser-produced spectrum shown in Fig. 1 compared with with synthetic spectra calculated at three values of the electron density.

where A_d is the area on the film of the densitometer slit, t is the time, V is the volume of plasma over which emission occurs, and (x, y) are spatial coordinates in the plane of the slit. In our calculations we have assumed that most of the emission from each ion occurs at the temperature of maximum abundance of the ion in ionization equilibrium. We adopt the values of fractional abundances for each ion (N_z/N_t) given by Landini and Fossi [6] at the equilibrium temperatures (with N_z being the ion number density and $N_t \equiv \Sigma N_z$ being the total number density of all the aluminum ions), and we assume equal emission measures for each ion; that is, we assume $\int N_e^2\, dV$ is the same for each ion. It is more desirable to determine N_j in Eq. (5) from computer codes that model the hydrodynamic expansion of the plasma, but this is beyond the scope of the present discussion.

To proceed further, it is necessary to construct a film-calibration curve. This can be done by comparing the relative intensities and photographic densities of lines close in

wavelength emitted by a common ion. The theoretical intensity ratios of these lines depend only on atomic excitation rates. Because the lines are close in wavelength, the instrumental efficiency is the same for all the lines. The film-calibration curve constructed in this manner is shown in Fig. 3.

With the curve in Fig. 3 relative intensities of all the lines in the foil spectrum can be determined. The relative intensities of all the unblended lines, and blends of lines emitted by a common ion, are given in Table 1. The intensities of the lines have been normalized to the intensity of the strong Al X resonance line at 332.78 Å. Also given in Table 1 are the normalized theoretical intensities for a density of 10^{20} cm^{-3}. This density is typical for the bright portions of the expanding plume of glass-laser-produced plasmas [5].

The experimental and theoretical intensities in Table 1 can be compared graphically. The theoretical and experimental intensity ratios of the same lines are plotted in Fig. 4 for all those lines which are not sensitive to precise values of N_e. Lines from the same ion are designated by common symbols. If the relative intensities of lines in the experimental and theoretical spectra were the same, the ratios would all be unity. Figure 4 shows that this is not the case.

Lines of the same ion define the solid curves indicated. The solid curves are eye estimates of the best fit to the data, with the shape of the curves being based on the theoretical shape given in Feldman et al. [1]. These curves have a simple interpretation. They define the instrumental efficiency. Thus, one important result of this type of analysis is that the instrumental efficiency of a spectrograph operating in this wavelength region can be determined. This is not an easy task using other experimental techniques.

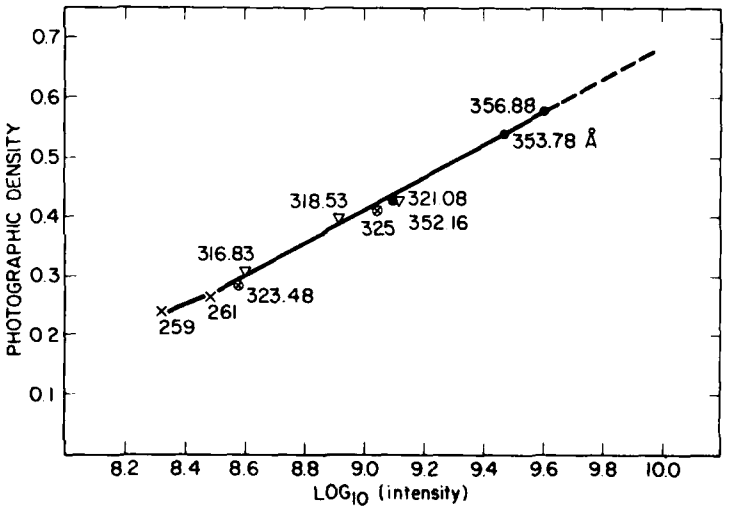

Fig. 3 — The film-calibration curve for the glass-laser spectrum

Table 1—Spectra of an aluminum-foil plasma produced by a Nd:glass laser

Ion	λ (Å)	Photo Density	$J_{expt.}$	$J_{theor.}$ ($N_e = 10^{20}$ cm^{-3})
Al VII	259*	0.24	0.035	1.3
Al VII	261*	0.26	0.050	1.3
Al VI	275.35	0.18	<0.033	0.78
Al IX	280.16	0.3†	0.067	0.45
Al V	281.40	0.33	0.085	3.4
Al IX	284.05	0.54	0.5	2.2
Al VIII	289	0.39	0.13	2.2
Al IX	300.60	0.30	0.067	0.31
Al IX	305.08	0.30	0.067	0.44
Al VI	312.24	0.44†	0.22	1.8
Al IX	316.83*	0.31	0.067	0.40
Al IX	318.53*	0.40	0.14	0.79
Al IX	321.08*	0.42	0.22	1.2
Al VIII	323.48*	0.29	0.063	0.24
Al VIII	325	0.42	0.18	0.76
Al VIII	331.10 331.07	0.23	0.035	0.21
Al X	322.78	0.62	1.0	1.0
Al VIII	334.52 334.55	0.34	0.090	0.42
Al VIII	340.23	0.20	≈0.027	0.48
Al VII	343.28 343.64	0.39	0.13	0.68
Al VII	352.16*	0.42	0.22	0.45
Al VII	353.78*	0.54	0.50	0.98
Al VII	356.88*	0.58	0.67	1.3
Al IX	385.03	0.42†	0.18	0.25
Al VII	386.03	0.22†	0.033	0.33
Al VII + Al IX	392.02 392.42	0.51	0.37	0.56
Al X	394.83	0.50†	0.33	0.47
Al IX + Al X	395.44 395.51	0.49†	0.32	0.42
Al X	397.85	0.39†	0.14	0.22
Al VIII	399.57	0.45	0.23	0.94
Al X	400.46	0.50†	0.33	0.16
Al X	401.18	0.59	0.73	0.80
Al X	403.60	0.32	0.075	0.21
Al X	406.35	0.41†	0.17	0.26

*Lines used to construct the film calibration curve.

†Blended lines.

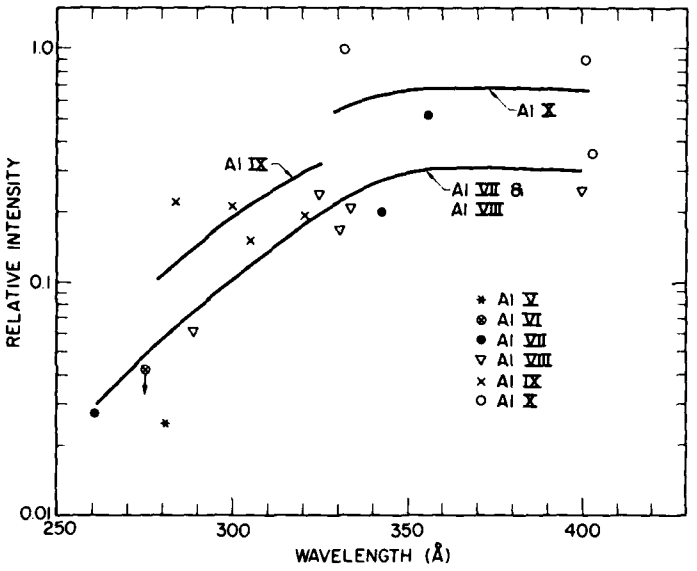

Fig. 4 — A comparison of the theoretical and experimental line intensities for the glass-laser-produced spectrum (Table 1). The solid curves define the instrumental efficiency as a function of wavelength.

If the assumptions used in constructing the theoretical spectra were correct, then all the solid curves would coincide. This is also not the case; the curves defined by the most highly ionized species fall above those of the lower ionized species. Only one line of Al V is available, and only an upper limit can be given for the Al VI line. The departures of the curves indicate a greater preponderance of higher temperature ions in the plasma than predicted by the simple equilibrium assumption and by the assumption of equal emission measures.

Since laser-produced plasmas appear to be transiently ionizing from the examination of time-averaged x-ray spectra [7], the departures in Fig. 4 are likely more severe than they appear. That is, not only are the relative ion abundances not given by their equilibrium values, but the temperatures at which the ions emit are probably higher than the equilibrium values. Implicit in our analysis is that the average temperature at which an ion emits over the lifetime of the plasma is the ionization equilibrium temperature. However, if the plasma were transiently ionizing, the line intensities of the less ionized species such as Al V would be increased relative to the more highly ionized species such as Al X.

Finally we note some scatter in the results for Al X. It is unclear whether this scatter is a reflection of a breakdown in the assumptions used to construct the theoretical spectra or is simply a result of local imperfections in the film or irregularities resulting from the film development process.

In summary, the preceding discussion shows how the film-calibration curve, the instrumental efficiency as a function of wavelength, and information on the relative ion abundances and their temperatures of formation in the plasma can be obtained using synthetic spectra coupled with monochromatic images of the plasma in different spectral lines. This last feature is the most important from the point of view of the physics of the plasma expansion. To gain more quantitative information from the spectra, it is necessary to incorporate the spectroscopic analysis as a subroutine in a general computer code that describes the hydromagnetic expansion of the plasma. This is feasible in light of the sophisticated codes that now exist at several laboratories. The primary purpose of the present discussion is to demonstrate the considerable potential of XUV image spectroscopy for diagnosing physical conditions in laser-produced plasmas and the importance of considering the entire spectrum rather than only a few lines.

MORPHOLOGY OF THE EXPANSION AND COMPARISON OF CO_2 AND FOIL SPECTRA

The relative intensities of the images in Fig. 1 between the CO_2-laser-produced thick-slab spectrum and the foil spectrum look similar. This is not surprising, for the following reasons. First, glass-laser plasma densities are around 10^{20} to 10^{21} cm^{-3}, whereas CO_2 plasma densities are around 10^{18} to 10^{19} cm^{-3}. However, within the density range from 10^{18} to 10^{21} cm^{-3} there are few density-sensitive line ratios in aluminum ions as compared with the situation for titanium or iron spectra. (In Refs. 5, 1, and 2 we discussed several density-sensitive ratios.) This is because the spontaneous decay rates in aluminum ions are substantially lower than corresponding rates in a heavier element such as iron. Also, the collisional excitation rates are smaller for iron ions than for aluminum ions. Second, the ions Al V through Al X are easily produced in both CO_2-laser-produced and glass-laser-produced plasmas; that is, their ionization potentials are significantly lower than the temperatures of these plasmas. Thus spectra from light elements such as aluminum are useful for investigating departures from ionization balance in plasmas produced by CO_2 laser and glass lasers but do not have much utility for determining electron density or maximum achieved electron temperature in the plasmas.

We discussed the morphology of the expansion of laser plasmas in Refs. 1 and 2. We noted that the plasma appears to expand in narrow conical plumes. The images of the more highly ionized ions, such as Fe XVI and Ca XVII, appear to form cylindrical plumes of smaller radius than is the case for less ionized species. This is most obvious by comparing the aluminum-plasma images produced by a CO_2 laser in Fig. 1 with the images in Fig. 5. The images in Fig. 5 are due to 2ℓ-$3\ell'$ and 2ℓ-$4\ell'$ transitions in the light ion C IV. The images fan out into large cone-shaped structures. This behavior for carbon was pointed out some time ago by Irons et al. [8], but the laser they used produced considerably lower power densities than the lasers under discussion here.

Small differences in the shapes of the expanding plumes of different aluminum ions can be seen in Fig. 1. For example, the Al VII image at 356.9 Å appears to fan outward into a larger cone than do the Al X images at 332.8 Å or 406.4 Å. The impression obtained from such comparisons is that the general shape of the expanding plasma is a cone, with the highest temperature region (more highly ionized species) occupying the center of the

Fig. 5 — Spectrum of a plasma produced from a solid planar carbon target by a CO_2 laser

cone. Lower temperature regions appear to form successive overlapping shells around the high-temperature region. Again, this temperature structure was found for carbon plasmas by Irons et al. [8]. The morphology for heavier elements appears to be similar, but the cones of the images of heavier ions appear almost cylindrical, and the temperature structure is correspondingly more difficult to discern.

REFERENCES

1. U. Feldman, G.A. Doschek, D.K. Prinz, and D.J. Nagel, J. Appl. Phys. 47, 1341 (1976).

2. G.A. Doschek, U. Feldman, P.G. Burkhalter, T. Finn, and W.A. Feibelman, J. Phys. B: Atom. Molec. Phys. 10, L745 (1977).

3. K.P. Dere, H.E. Mason, K.G. Widing, and A.K. Bhatia, Astrophys. J. 40, 341 (1979).

4. U. Feldman, G.A. Doschek, and W.E. Behring, Space Science Rev. 22, 191 (1978).

5. G.A. Doschek, U. Feldman, J. Davis, and R.D. Cowan, Phys. Rev. A 12, 980 (1975).

6. M. Landini and B. C. Monsignori Fossi, Astron. and Astrophys. Suppl. 7, 291 (1972).

7. V.A. Boiko, A. Ya. Faenov, and S.A. Pikuz, J. Quant. Spectrosc. Radiat. Transfer 19, 11 (1978).

8. F.E. Irons, R.W.P. McWhirter, and N.J. Peacock, J. Phys. B: Atom. Molec. Phys. 5, 1975 (1972).